

A 3-D Quasi-Zero-Stiffness-Based Sensor System for Absolute Motion Measurement and Application in Active Vibration Control

Xiuting Sun, Xingjian Jing, *Member, IEEE*, Li Cheng, and Jian Xu

Abstract—A novel 3-D quasi-zero-stiffness (3DQZS) system is proposed to construct a 3-D sensor system for absolute motion measurement in vibration systems. The 3DQZS system is achieved by employing a predeformed scissor-like structure. With mathematical modeling and the harmonic balance method, the nonlinear dynamic response of the 3-D sensor system is deeply analyzed. It is shown that this novel 3DQZS-based sensor system is very effective and reliable in 3-D absolute motion measurement in vibration systems. A case study in active vibration control using the proposed 3-D sensor indicates that much better vibration control performance can be readily achieved compared with conventional methods using a similar linear feedback controller. This novel sensor system should provide an alternative or much better solution to many vibration control problems in various engineering practices.

Index Terms—Active vibration control, nonlinear system, quasi-zero stiffness (QZS), scissor-like structure (SLS), vibration sensor.

I. INTRODUCTION

IN VARIOUS engineering practices for system identification [1]–[3], control [4]–[12], [31]–[33], and filter design [13], [14], system state measurement or estimation has always been a critical task because the control of vibration platforms (e.g., vehicle suspension, instrument protection in ships or UAV, etc.) usually requires accurate knowledge of full system states with respect to a global coordinate system in active/semiactive control for better vibration suppression performance [9]–[12]. Therefore, various mechatronic systems are introduced as sensors for motion measurement [15]–[19]. For measurement of absolute displacement or velocity, although some advanced measurement technology could be applied such as inertial sensors [15], radars or laser technology [16]–[19], etc., realistic issues

related to accuracy, installation and/or development cost would have to be considered. Accelerometers are often applied to measure absolute acceleration in a vibrating system. But absolute motion of a system could not be accurately recovered from acceleration signals. Although some existing algorithms (e.g., linear filters) could be used to estimate unmeasured states (e.g., displacement) from measured ones (e.g., acceleration), it would induce problems to control systems such as time delay due to computation cost. It is known that time delay could easily deteriorate the stability of a dynamic system and bring complexity for analysis and design [20]–[23]. Even though for some cases [24]–[26] in vibration absorbers, time delay could benefit vibration suppression when absolute displacement can be used in feedback control, the value of the time delay should be set in certain critical ranges with the help of precise instruments such as signal amplification and readout devices.

In order to conveniently and accurately measure absolute motion for vibration control of vibration systems such as vehicle suspension systems or instrument protection in ships or UAV, etc., a novel three-direction sensor (3DS) system is proposed in this study. The sensor is designed by employing a novel 3-D quasi-zero-stiffness (3DQZS) vibration isolation system. The latter can achieve excellent passive nonlinear vibration isolation using a predeformed scissor-like structure, and this scissor-like structure was shown to be an excellent quasi-zero-stiffness (QZS) system recently in [27]. Different from existing QZS vibration isolators in [28]–[30] effective only for one-direction (typically composed by two horizontal precompression springs and a vertical spring), the proposed 3DQZS system is constructed by two horizontal scissor-like structures (SLSs) with predeformation and vertical springs, which can realize QZS property in three directions. Because of this remarkable advantage of the 3DQZS system, the relative motion between the 3DQZS system and the base structure can be sufficiently close to the absolute motion of the base structure. Moreover, the stiffness characteristics and geometric parameters of the 3DQZS system can be easily designed and adjusted so as to greatly increase measurement accuracy in three directions. The proposed 3-D sensor is easy to design and implement in practice and some problems as mentioned above (e.g., time delay, high cost) could be reasonably avoided. Besides theoretical analysis, a case study in active vibration control using this novel sensor vindicates the effectiveness.

The rest of the paper is organized as follows. The structure of the novel 3-D sensor system is introduced in Section II which is modeled through the Lagrange principle [34]. Then, relative

Manuscript received March 7, 2014; revised June 20, 2014; accepted June 25, 2014. Date of publication August 6, 2014; date of current version October 3, 2014. Recommended by Technical Editor M. Iwasaki. This work was supported in part by the National Natural Science Foundation of China (No. 61374041), in part by the GRF projects of HK RGC (15206514, 517810), and in part by the internal Research Grants of The Hong Kong Polytechnic University. (Corresponding author: Xingjian Jing).

X. Sun is with the Department of Mechanical Engineering, The Hong Kong Polytechnic University, Hung Hom, Hong Kong, and also with the School of Aerospace Engineering and Applied Mechanics, Tongji University, Shanghai 200092, China (e-mail: 05mech_sunxiuting@tongji.edu.cn).

X. Jing is with the Department of Mechanical Engineering, The Hong Kong Polytechnic University, Hung Hom, Hong Kong, and also with The Hong Kong Polytechnic University Shenzhen Research Institute, Shenzhen 518057, China (e-mail: mmjxj@polyu.edu.hk; xingjian.jing@gmail.com).

L. Cheng is with the Department of Mechanical Engineering, The Hong Kong Polytechnic University, Hung Hom, Hong Kong.

J. Xu is with School of Aerospace Engineering and Applied Mechanics, Tongji University, Shanghai 200092, China.

Digital Object Identifier 10.1109/TMECH.2014.2338932

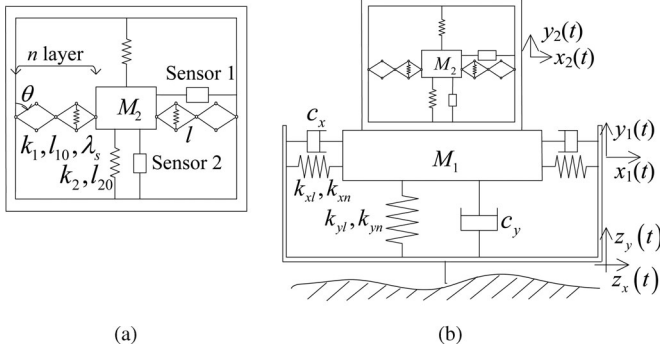


Fig. 1. Structural diagram of (a) the proposed absolute motion sensor and (b) its application to a vibration system.

motion is compared to absolute motion of the vibration mass for different base excitations. A method for signal rectification for accuracy improvement is discussed in Section IV. Section V shows an application of the novel sensor in feedback control. A conclusion is drawn thereafter.

II. THREE-DIMENSIONAL SENSOR SYSTEM AND ITS MODELING

A. Structure of the Sensor System

Fig. 1(a) is the proposed 3-D sensor which can be used to measure absolute motion of a vibration system in three different directions. In the structure of the 3-D sensor, M_2 is a small mass which includes the mass of two relative motion Sensors 1 and 2. The mass M_2 is connected to two n -layer SLSs with springs whose stiffness is k_1 and original length is l_{10} . And two vertical springs whose stiffness is k_2 and original length is l_{20} .

Fig. 1(b) shows the structural diagram of the 3-D sensor used in a vibration platform with mass M_1 . The vibration platform is supposed to be connected to the base with horizontal springs whose linear stiffness is k_{xl} and nonlinear stiffness k_{xn} , vertical springs whose linear stiffness is k_{yl} and nonlinear stiffness k_{yn} , and two dampers with damping coefficients c_x and c_y . All the structural parameters and their default values are listed in Table I in the Appendix. Without loss of speciality, the base excitations are supposed in horizontal direction $z_x(t)$ and vertical direction $z_y(t)$. The absolute vibration displacements of mass M_1 are denoted by $x_1(t)$ and $y_1(t)$, respectively. Similarly, the absolute vibration displacements of the mass M_2 are denoted by $x_2(t)$ and $y_2(t)$. Sensors 1 and 2 are the two relative motion sensors whose signals obtained are the relative motions (displacement/velocity) between the mass M_2 and M_1 for two directions. The variables of the system in Fig. 1 are listed in Table II in the Appendix.

B. Geometrical Relations

In order to model this dynamic system to obtain relative and absolute motion, the geometrical relations and deformations of each spring and component in the system should be analyzed. Fig. 2 is the right-side SLS in the 3-D sensor.

Fig. 2 shows the deformation of the right-side SLS in the 3-D sensor. After deformation, the length of the spring in the

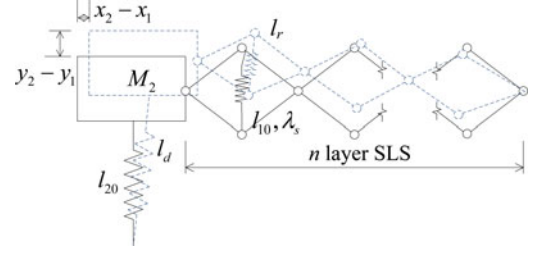


Fig. 2. Deformations of springs and SLSs in the 3-D sensor in vibration.

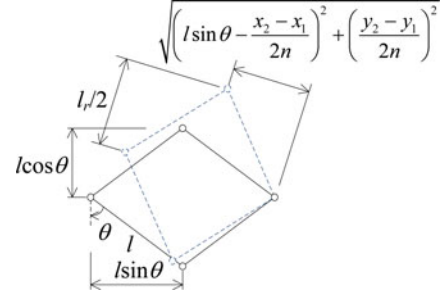


Fig. 3. Deformation of one layer in the right SLS in the sensor.

right-side SLS is defined as l_r and the length of the spring in the left-side SLS is defined as l_l . The deformation of the upper vertical spring in the 3-D sensor is defined as l_u , and the lower vertical spring is l_d . Fig. 3 is the geometrical relation of one layer in the right-side SLS in vibration.

As shown in Fig. 3, the deformation of the right-side spring l_r can be obtained from the corresponding geometrical relation. Similar to the deformation l_r , the deformation of the spring in the left-side SLS in the sensor l_l also can be obtained from the geometrical relation, and the values of the deformations l_l and l_r of the two springs are as follows:

$$l_l = 2\sqrt{l^2 - \frac{(2nl \sin \theta + x_2 - x_1)^2 + (y_2 - y_1)^2}{4n^2}} \quad (1)$$

$$l_r = 2\sqrt{l^2 - \frac{(2nl \sin \theta - x_2 + x_1)^2 + (y_2 - y_1)^2}{4n^2}} \quad (2)$$

and similar to the left- and right-SLSs in the sensor, the deformations of the upper and lower springs are defined as l_u and l_d , which are given by

$$l_u = \sqrt{(l_{20} - y_2 + y_1)^2 + (x_2 - x_1)^2} \quad (3)$$

$$l_d = \sqrt{(l_{20} + y_2 - y_1)^2 + (x_2 - x_1)^2}. \quad (4)$$

Then, the dynamic equation of the system in Fig. 1(b) can be obtained by Lagrange principle, which is derived in the next section.

C. Modeling

The absolute motions x_1 , y_1 , x_2 and y_2 of mass M_1 and M_2 are chosen as the generalized coordinates. The kinetic energy T

of the system is

$$T = \frac{1}{2}M_1\dot{x}_1^2 + \frac{1}{2}M_1\dot{y}_1^2 + \frac{1}{2}M_2\dot{x}_2^2 + \frac{1}{2}M_2\dot{y}_2^2. \quad (5)$$

Potential energy V is expressed as

$$\begin{aligned} V = & \frac{1}{2}k_{yl}(y_1 - z_y)^2 + \frac{1}{4}k_{yn}(y_1 - z_y)^4 + k_{xl}(x_1 - z_x)^2 \\ & + \frac{1}{2}k_{xn}(x_1 - z_x)^4 + \frac{1}{2}k_1(l_l - l_{10})^2 + \frac{1}{2}k_1(l_r - l_{10})^2 \\ & + \frac{1}{2}k_2(l_d - l_{20})^2 + \frac{1}{2}k_2(l_u - l_{20})^2 \end{aligned} \quad (6)$$

where it has $l_{10} + \lambda_s = 2l \cos \theta$ because of the geometric condition before deformation in SLSS. The Lagrange principle [34] of the two-direction vibration in the system of Fig. 1(b) is

$$\begin{cases} \frac{d}{dt} \left(\frac{\partial L}{\partial \dot{x}_1} \right) + \frac{\partial L}{\partial x_1} = Q_{x_1} \\ \frac{d}{dt} \left(\frac{\partial L}{\partial \dot{y}_1} \right) + \frac{\partial L}{\partial y_1} = Q_{y_1} \\ \frac{d}{dt} \left(\frac{\partial L}{\partial \dot{x}_2} \right) + \frac{\partial L}{\partial x_2} = Q_{x_2} \\ \frac{d}{dt} \left(\frac{\partial L}{\partial \dot{y}_2} \right) + \frac{\partial L}{\partial y_2} = Q_{y_2} \end{cases} \quad (7)$$

where L in the Lagrange equation is given by $L = T - V$; Q_{x_1} , Q_{y_1} , Q_{x_2} , and Q_{y_2} are the generalized forces in the four coordinates which reflects the effect of linear dampers. Therefore, the dynamic equations of the four generalized coordinates are as follows:

$$\begin{aligned} M_1\ddot{x}_1 + 2k_{xl}\dot{x}_1 + 2k_{xn}\dot{x}_1^3 + k_1 \left(\frac{\lambda_s \sec^3 \theta}{ln^2} - \frac{2 \tan^2 \theta}{n^2} \right) \dot{x}_2 \\ + 2c_x\dot{x}_1 + \left[\frac{2k_2}{l_{20}^2} - \frac{k_1(2l \cos \theta - \lambda_s)(2 - \cos 2\theta) \sec^5 \theta}{8l^3 n^4} \right] \dot{x}_2 \dot{y}_2^2 \\ + \left[k_1 \sec^6 \theta \left(\frac{3 - 2 \cos 2\theta}{4l^2 n^4} \right) \left(\frac{\lambda_s \sec \theta - 2l}{2l} \right) - \frac{k_2}{l_{20}^2} \right] \dot{x}_2^3 \\ = -M_1\ddot{z}_x \end{aligned} \quad (8)$$

$$\begin{aligned} M_1\ddot{y}_1 + k_{yl}\dot{y}_1 + k_{yn}\dot{y}_1^3 + \left(\frac{k_1\lambda_s \sec \theta}{ln^2} - 2k_2 \right) \dot{y}_2 \\ + c_y\dot{y}_1 + \left[\frac{2k_2}{l_{20}^2} - \frac{k_1(2l \cos \theta - \lambda_s)(2 - \cos 2\theta) \sec^5 \theta}{8l^3 n^4} \right] \dot{x}_2^2 \dot{y}_2 \\ + \frac{k_1 \sec^2 \theta}{4l^2 n^4} \left(\frac{\lambda_s \sec \theta}{2l} - 1 \right) \dot{y}_2^3 = -M_1\ddot{z}_y \end{aligned} \quad (9)$$

$$\begin{aligned} M_2(\ddot{x}_1 + \ddot{x}_2) + k_1 \left(\frac{2 \tan^2 \theta}{n^2} - \frac{\lambda_s \sec^3 \theta}{ln^2} \right) \dot{x}_2 \\ + \left[-\frac{2k_2}{l_{20}^2} + \frac{k_1(2l \cos \theta - \lambda_s)(2 - \cos 2\theta) \sec^5 \theta}{8l^3 n^4} \right] \dot{x}_2 \dot{y}_2^2 \\ + \left[\frac{k_2}{l_{20}^2} - k_1 \sec^6 \theta \left(\frac{3 - 2 \cos 2\theta}{4l^2 n^4} \right) \left(\frac{\lambda_s \sec \theta}{2l} - 1 \right) \right] \dot{x}_2^3 \\ = -M_2\ddot{z}_x \end{aligned} \quad (10)$$

$$\begin{aligned} M_2(\ddot{y}_1 + \ddot{y}_2) + \left(2k_2 - \frac{k_1\lambda_s \sec \theta}{ln^2} \right) \dot{y}_2 \\ + \left[\frac{k_1(2l \cos \theta - \lambda_s)(2 - \cos 2\theta) \sec^5 \theta}{8l^3 n^4} - \frac{2k_2}{l_{20}^2} \right] \dot{x}_2^2 \dot{y}_2 \\ + \frac{k_1 \sec^2 \theta}{4l^2 n^4} \left(1 - \frac{\lambda_s \sec \theta}{2l} \right) \dot{y}_2^3 = -M_2\ddot{z}_y \end{aligned} \quad (11)$$

where $\hat{x}_1, \hat{y}_1, \hat{x}_2, \hat{y}_2$ are the relative motions which are expressed as $\hat{x} = \hat{x}_1 - z_x$, $\hat{y}_1 = y_1 - z_y$, $\hat{x}_2 = x_2 - x_1$, $\hat{y}_2 = y_2 - y_1$, and $z_x = z_{x0} \cos \omega t$ and $z_y = z_{y0} \cos \omega t$ for harmonic base excitation. Introducing the dimensionless transform, the dimensionless parameters of the system are chosen as

$$\begin{aligned} \omega_0 = \sqrt{\frac{k_{xl}}{M_1}}, \quad t' = \omega_0 t, \quad \gamma_x = \frac{k_{xn}}{k_{xl}}, \quad \xi_x = \frac{c_x}{2\sqrt{M_1 k_{xl}}}, \\ \omega_y = \sqrt{\frac{k_{yl}}{k_{xl}}}, \quad \gamma_y = \frac{k_{yn}}{k_{xl}}, \quad \xi_y = \frac{c_y}{2\sqrt{M_1 k_{xl}}}, \quad \gamma_1 = \frac{k_1}{k_{xl}}, \\ \gamma_2 = \frac{k_2}{k_{xl}}, \quad \mu = \frac{M_1}{M_2}, \quad \Omega = \frac{\omega}{\omega_0}. \end{aligned} \quad (12)$$

The default values of the dimensionless parameters are listed in Table III in the Appendix. Then, the dimensionless dynamic equation of the system is given by

$$\begin{aligned} \hat{x}_1'' + 2\hat{x}_1 + 2\gamma_x \hat{x}_1^3 + \gamma_1 \left(\frac{\lambda_s \sec^3 \theta}{ln^2} - \frac{2 \tan^2 \theta}{n^2} \right) \hat{x}_2 + 4\xi_x \hat{x}_1' \\ + \left[\gamma_1 \sec^6 \theta \left(\frac{3 - 2 \cos 2\theta}{4l^2 n^4} \right) \left(\frac{\lambda_s \sec \theta}{2l} - 1 \right) - \frac{\gamma_2}{l_{20}^2} \right] \hat{x}_2^3 \\ + \left[\frac{2\gamma_2}{l_{20}^2} - \frac{\gamma_1(2l \cos \theta - \lambda_s)(2 - \cos 2\theta) \sec^5 \theta}{8l^3 n^4} \right] \hat{x}_2 \hat{y}_2^2 \\ = -z_x'' \end{aligned} \quad (13)$$

$$\begin{aligned} \hat{y}_1'' + \omega_y^2 \hat{y}_1 + \gamma_y \hat{y}_1^3 + \left(\frac{\gamma_1 \lambda_s \sec \theta}{ln^2} - 2\gamma_2 \right) \hat{y}_2 + 2\xi_y \hat{y}_1' \\ + \left[\frac{2\gamma_2}{l_{20}^2} - \frac{\gamma_1(2l \cos \theta - \lambda_s)(2 - \cos 2\theta) \sec^5 \theta}{8l^3 n^4} \right] \hat{x}_2^2 \hat{y}_2 \\ + \frac{\gamma_1 \sec^2 \theta}{4l^2 n^4} \left(\frac{\lambda_s \sec \theta}{2l} - 1 \right) \hat{y}_2^3 = -z_y'' \end{aligned} \quad (14)$$

$$\begin{aligned} \hat{x}_1'' + \hat{x}_2'' + \mu \left[\frac{\gamma_2}{l_{20}^2} - \gamma_1 \sec^6 \theta \left(\frac{3 - 2 \cos 2\theta}{4l^2 n^4} \right) \right. \\ \left. \left(\frac{\lambda_s \sec \theta}{2l} - 1 \right) \right] \hat{x}_2^3 \\ + \mu \left[\frac{\gamma_1(2l \cos \theta - \lambda_s)(2 - \cos 2\theta) \sec^5 \theta}{8l^3 n^4} - \frac{2\gamma_2}{l_{20}^2} \right] \hat{x}_2 \hat{y}_2^2 \\ + \mu \gamma_1 \left(\frac{2 \tan^2 \theta}{n^2} - \frac{\lambda_s \sec^3 \theta}{ln^2} \right) \hat{x}_2 = -z_x'' \end{aligned} \quad (15)$$

$$\begin{aligned}
& \hat{y}_1'' + \hat{y}_2'' + \mu \left(2\gamma_2 - \frac{\gamma_1 \lambda_s \sec \theta}{ln^2} \right) \hat{y}_2 \\
& + \mu \left[\frac{\gamma_1 (2l \cos \theta - \lambda_s) (2 - \cos 2\theta) \sec^5 \theta}{8l^3 n^4} - \frac{2\gamma_2}{l_{20}^2} \right] \hat{x}_2^2 \hat{y}_2 \\
& + \frac{\mu \gamma_1 \sec^2 \theta}{4l^2 n^4} \left(1 - \frac{\lambda_s \sec \theta}{2l} \right) \hat{y}_2^3 = -z_y'' \quad (16)
\end{aligned}$$

where $(\cdot)'' = d^2(\cdot)/dt^2$, $\frac{d^2(\cdot)}{dt^2}$, $(\cdot)' = d(\cdot)/dt$, $\frac{d(\cdot)}{dt}$, and $z_x'' = -\Omega^2 z_{x0} \cos \Omega t'$, $z_y'' = -\Omega^2 z_{y0} \cos \Omega t'$ for harmonic base excitation.

III. DYNAMIC RESPONSE OF THE SENSOR SYSTEM

A. Selection of Structural Parameters

The signals measured by Sensors 1 and 2 are defined, respectively, as

$$g_1(\hat{x}_2) = \hat{x}_2 = x_2 - x_1 \quad (17)$$

$$g_2(\hat{y}_2) = \hat{y}_2 = y_2 - y_1. \quad (18)$$

From (17) and (18), the signals measured by Sensors 1 and 2 are linear functions of \hat{x}_2 which is the relative motion from M_2 to M_1 . Because the 3-D sensor can achieve 3DQZS property when the amplitude of x_2 is close to zero, the signals measured by Sensors 1 and 2 are as $g_1 \approx -x_1$ and $g_2 \approx -y_1$, respectively. Then, the signals measured for different directions can describe the absolute motion of M_1 .

As the signals measured by Sensors 1 and 2 are expected to represent the absolute motion of M_1 , the smaller amplitude of x_2 leads to more accuracy of the measured signals to the absolute motion. From the dimensionless dynamic equations in (15) and (16) for mass M_2 , the equivalent dimensionless linear stiffness for M_2 in x - and y -directions are given by

$$\begin{cases} K_x = \mu \gamma_1 \left(\frac{2 \tan^2 \theta}{n^2} - \frac{\lambda_s \sec^3 \theta}{ln^2} \right) \\ K_y = \mu \left(2\gamma_2 - \frac{\gamma_1 \lambda_s \sec \theta}{ln^2} \right). \end{cases} \quad (19)$$

As the values of K_x and K_y are close to zero, the 3DQZS property can be obtained. The parameters in (19) contain stiffness of springs γ_1 , γ_2 , structural parameters of SLSs l , n , θ and the predeformation of the springs in SLSs λ_s . The structural parameters λ_s and θ can be adjusted more easily than γ_1 , γ_2 , l , and n . To achieve $K_x = K_y = 0$, the value of λ_s and θ can be chosen as

$$\begin{cases} \lambda_s = \frac{2l \tan^2 \theta}{\sec^3 \theta} \\ \theta = \arcsin \left(n \sqrt{\frac{\gamma_2}{\gamma_1}} \right) = \arcsin \left(n \sqrt{\frac{k_2}{k_1}} \right). \end{cases} \quad (20)$$

With the values of equivalent stiffness K_x and K_y close to zero, the signals measured can precisely describe the absolute motion of M_1 in a large frequency domain.

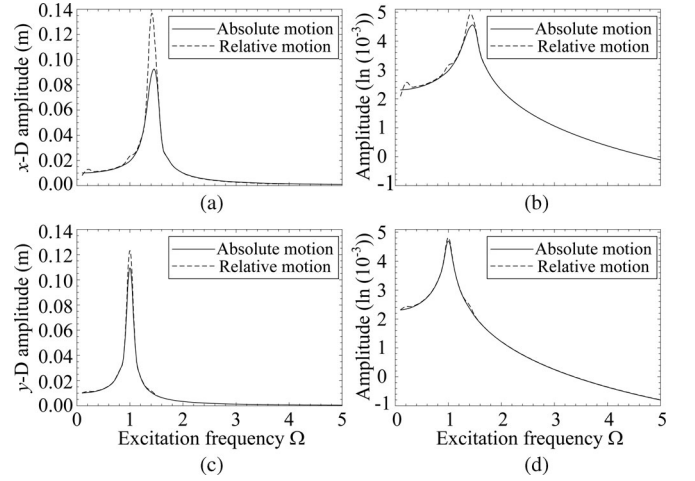


Fig. 4. Comparisons of amplitudes between absolute motion $-x_1$, $-y_1$ and relative motion \hat{x}_2 , \hat{y}_2 , of the 3-D sensor for periodic excitation. Plots (a) and (b) are comparisons in x -direction (x -D), and (c) and (d) are comparisons in y -direction (y -D).

B. Periodic Excitation

From the dimensionless dynamic equations (13)–(16), it is obvious that the stiffness and damping properties are nonlinear functions of motion and velocity, and the natural frequencies (17) of the horizontal and vertical vibrations are dependent on the structural parameters of the system. The harmonic balance method is utilized to solve the motions in two-dimensional vibrations. The solutions of \hat{x}_1 , \hat{y}_1 , \hat{x}_2 , and \hat{y}_2 are denoted as

$$\begin{cases} \hat{x}_1(t') = a_{x1} \cos(\Omega t' + \phi_{x1}) \\ \hat{y}_1(t') = b_{y1} \cos(\Omega t' + \phi_{y1}) \\ \hat{x}_2(t') = a_{x2} \cos(\Omega t' + \phi_{x2}) \\ \hat{y}_2(t') = b_{y2} \cos(\Omega t' + \phi_{y2}) \end{cases} \quad (21)$$

where a_{x1} , b_{y1} , a_{x2} , and b_{y2} are the amplitudes of the first harmonic vibrations of the system; ϕ_{x1} , ϕ_{y1} , ϕ_{x2} , and ϕ_{y2} are the phases. The amplitude of x -direction excitation is z_{x0} and y -direction excitation is z_{y0} .

For the values of structural parameters shown in Table I, as $k_1 = 300 \text{ N}\cdot\text{m}^{-1}$, $k_2 = 100 \text{ N}\cdot\text{m}^{-1}$, $n = 1$, $l = 0.2 \text{ m}$ for the SLSs in the proposed 3-D sensor, the equivalent linear stiffness K_x and K_y of the sensor are zero as $\lambda_s = 0.109 \text{ m}$ and $\theta = 0.6155 \text{ rad}$. The amplitudes and phases of relative motions can also be obtained by the harmonic balance method. Comparisons of the amplitudes and phases between the signals measured by the 3-D sensor, \hat{x}_2 , \hat{y}_2 and the absolute motion $-x_1$, $-y_1$ of mass M_1 are shown in Figs. 4 and 5.

From Fig. 4, it can be seen that in a wide frequency range, the difference of the relative motion of M_1 with respect to M_2 and the absolute motion of M_1 is very small. Because the accuracy between the measured signals and the absolute motions is dependent on the vibration isolation effectiveness of the structures within the sensor system, the response of M_2 is the difference between the measured signals of the proposed sensor and the absolute motions. Figs. 4 and 5 show that in the natural

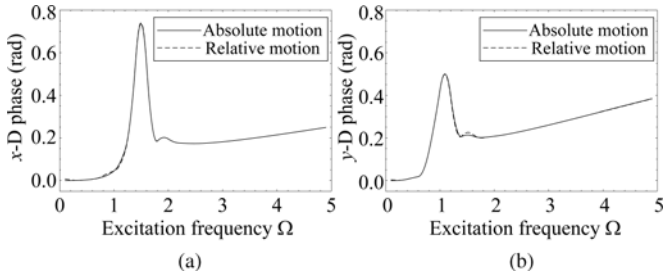


Fig. 5. Phases of absolute motion $-x_1, -y_1$ and relative motion, \hat{x}_2, \hat{y}_2 . Plot (a) is in x -direction and (b) is in y -direction.

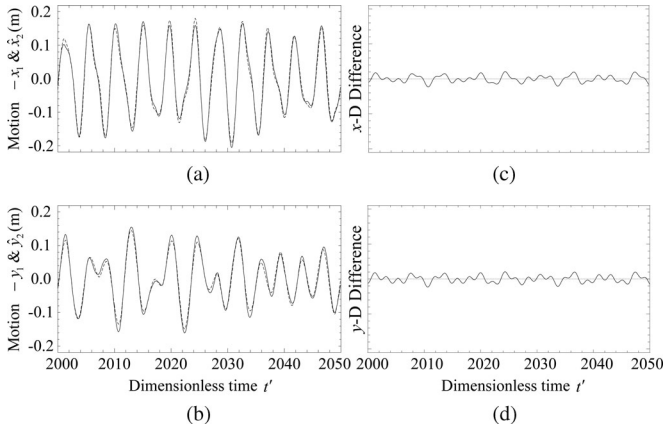


Fig. 6. Relative motion \hat{x}_2, \hat{y}_2 (lines) and absolute motion $-x_1, -y_1$ (dashed lines) for multiperiodic excitation in (a) x -direction and (b) in y -direction; plot (c) is the difference between \hat{x}_2 and $-x_1$, and (d) is the difference between \hat{y}_2 and $-y_1$.

frequency and ultralow frequency domain, there is error between the relative motion and absolute motion. And around the natural frequency of M_1 , the vibration of mass M_2 is excited by x_1 whose amplitude is large, thus the vibration amplitude of x_2 cannot reach zero. Although the equivalent linear stiffness of the proposed sensor is set to zero, the nonlinearity cannot be ignored which induces the offset of resonance peak from zero to the right side of the response of M_2 . Thus, for the range of ultralow frequency domain, the vibration of mass M_2 is around resonance peak which results in the error between the relative motion and the absolute motion. Also, from Fig. 5, it can be seen that the phase of the relative motion is very close to the absolute motion.

Therefore, it can be summarized that through choosing appropriate structural parameters in the proposed 3-D sensor, under harmonic excitation, the relative motion in x - and y -direction measured by Sensors 1 and 2 can reflect the absolute motion of the mass M_1 in a wide frequency range.

C. Multiperiodic Excitation

Fig. 6 is the comparison of the absolute motion and the relative motion of M_1 for multiperiodic excitation $z_x(t)$ and $z_y(t)$ which are for example $z_x(t) = 0.01\cos(1.1t) + 0.005\cos(1.6t) + 0.008\cos(3t)$ and $z_y(t) = 0.012\cos(1.1t) + 0.007\cos(1.6t) + 0.006\cos(3t)$. Similar conclusions can be

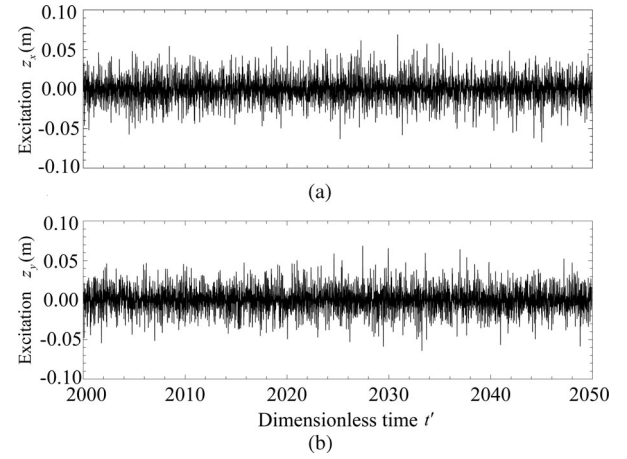


Fig. 7. Time series diagram of random base excitation. Plot (a) is $z_x(t)$ and (b) is $z_y(t)$.

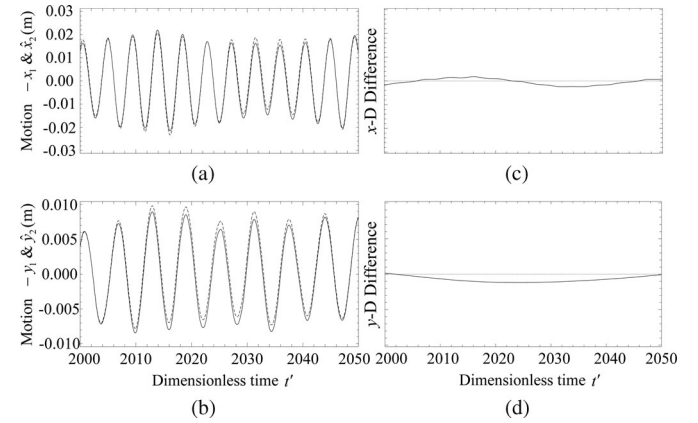


Fig. 8. Relative motion, \hat{x}_2, \hat{y}_2 (lines) and absolute motion $-x_1, -y_1$ (dashed lines) for random excitation in (a) x -direction and (b) in y -direction. Plot (c) is the difference between \hat{x}_2 and $-x_1$, and (d) is the difference between \hat{y}_2 and $-y_1$.

drawn for other multiperiodic excitation. The structural parameters in the system are chosen as Table I. Fig. 6 clearly shows that the magnitudes of the amplitude in x - and y -direction are in the order of 0.2 while the magnitudes of the difference are less than 0.01. Therefore, the relative motions measured by the 3-D sensor can also describe the absolute motion of M_1 for multiperiodic base excitation because of the excellent isolation effectiveness by using the SLSSs.

D. Random Excitation

Fig. 7 is the random excitation $z_x(t)$ and $z_y(t)$, and Fig. 8 is the comparison of the absolute motion $-x_1$ and $-y_1$ of M_1 and its relative motion \hat{x}_2 and \hat{y}_2 . The structural parameters in the system are still chosen as Table I.

From Fig. 8, it can be seen that the absolute motion of M_1 is very close to the relative motion between M_2 and M_1 . For x -direction, the amplitude of the response of the vibration object is about 0.02 while the maximum difference between $\hat{x}_2 - x_1$ is only about 0.002, and for y -direction, the response is about 0.01 and the difference is less than 0.001. This is exactly consistent with the conclusions made for other types of excitations above.

E. Signal Rectification for High Accuracy

As the results already shown, there are some errors between the relative motion (measured) and the absolute motion of M_1 which are induced by the vibration of M_2 . For periodic excitation, the relative motion signals measured can be rectified to approach the absolute motion of M_1 based on the analysis of displacement transmissibility from M_1 to M_2 . As the displacement transmissibility in x -direction is T_x and y -direction is T_y , which are given by

$$\begin{cases} T_x = \frac{\|x_2\|}{\|x_1\|} = \frac{\|\hat{x}_2 + \hat{x}_1 + z_x\|}{\|\hat{x}_1 + z_x\|} \\ T_y = \frac{\|y_2\|}{\|y_1\|} = \frac{\|\hat{y}_2 + \hat{y}_1 + z_y\|}{\|\hat{y}_1 + z_y\|} \end{cases} \quad (22)$$

For harmonic excitation, substituting the expressions of solutions and excitations z_x and z_y into (14), it is obtained that T_x and T_y can be described as

$$T_x = \sqrt{1 + \frac{a_{x2}^2 + 2a_{x1}a_{x2} \cos(\phi_{x1} - \phi_{x2}) + 2a_{x2}z_{x0} \cos \phi_{x2}}{a_{x1}^2 + 2a_{x1}z_{x0} \cos \phi_{x1} + z_{x0}^2}} \quad (23)$$

$$T_y = \sqrt{1 + \frac{a_{y2}^2 + 2a_{y1}a_{y2} \cos(\phi_{y1} - \phi_{y2}) + 2a_{y2}z_{y0} \cos \phi_{y2}}{a_{y1}^2 + 2a_{y1}z_{y0} \cos \phi_{y1} + z_{y0}^2}} \quad (24)$$

The signal measured by Sensors 1 and 2 are as $g_1(\hat{x}_2) = \hat{x}_2 = x_2 - x_1$ and $g_2(\hat{y}_2) = \hat{y}_2 = y_2 - y_1$. Because of the displacement transmissibility from M_1 to M_2 can be obtained by (17) and (18), the amplitude of the relative motion signals measured can thus be corrected to approach the amplitude of the absolute motion of M_1 . The amplitude of the signals measured can be expressed as

$$\|g_1(\hat{x}_2)\| = \|\hat{x}_2\| = \sqrt{\|x_2 - x_1\|^2} = |1 + T_x| \|x_1\| \quad (25)$$

$$\|g_2(\hat{y}_2)\| = \|\hat{y}_2\| = \sqrt{\|y_2 - y_1\|^2} = |1 + T_y| \|y_1\|. \quad (26)$$

Therefore, the corrected amplitudes of the absolute motion of M_1 are

$$\begin{cases} \|x_1\| = \frac{\|g_1(\hat{x}_2)\|}{|1 + T_x|} = \frac{\|\hat{x}_2\|}{|1 + T_x|} \\ \|y_1\| = \frac{\|g_2(\hat{y}_2)\|}{|1 + T_y|} = \frac{\|\hat{y}_2\|}{|1 + T_y|} \end{cases} \quad (27)$$

In the effective isolation frequency range of the 3DQZS system, both T_x and T_y are near to zero in (27), and thus the amplitude of the absolute motion of M_1 can be precisely obtained by (17). For the equivalent stiffness of the proposed sensor structure is close to zero in different vibration directions and the natural frequency is close to zero, the effective isolation frequency range of the 3DQZS is very large. Therefore, in a wide frequency range, the relative signal measured by Sensors 1 and 2 can be very close to the absolute motion of M_1 .

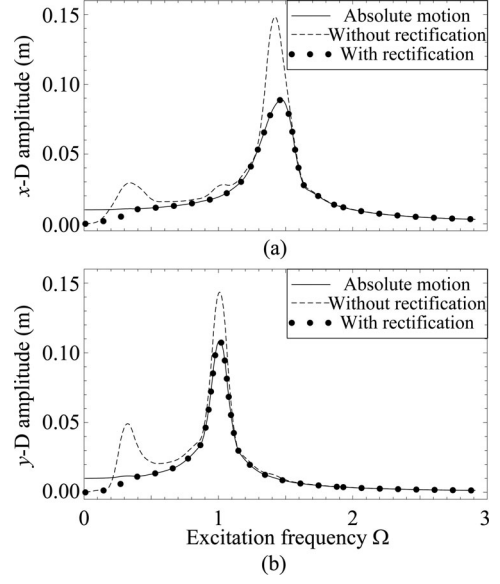


Fig. 9. Comparison among the absolute motion $-x_1, -y_1$, relative motion, \hat{x}_2, \hat{y}_2 , and corrected absolute motion via (27) for harmonic excitation. Plot (a) is the comparison in x -direction and (b) in y -direction.

At the resonance peak, the relative motions around natural frequency are not so close to the absolute ones, the rectification calculation (27) can be used at the natural frequency. Moreover, for example, if the structural parameters take $k_1 = 300 \text{ N}\cdot\text{m}^{-1}$, $k_2 = 100 \text{ N}\cdot\text{m}^{-1}$, $n = 1$, $l = 0.2 \text{ m}$, $\lambda_s = 0.1 \text{ m}$ and $\theta = 0.6 \text{ rad}$ in SLSs, the zero-stiffness conditions $K_x = 0$ and $K_y = 0$ cannot be satisfied. In this case, the relative motions measured may have some deviation from the absolute motions of M_1 . However, with the rectification method proposed in (27), the amplitudes of the relative motions measured are sufficiently close to the absolute motions of M_1 which is shown in Fig. 9. For the harmonic input, the difference between the measured signals and the absolute motions can be eliminated because T_x and T_y can be known or computed accurately at each frequency.

IV. APPLICATION IN ACTIVE VIBRATION CONTROL WITH A SIMPLE LINEAR FEEDBACK

The proposed 3-D sensor can be used to provide absolute motion states of a system in feedback vibration control. An example can be seen in Fig. 10(a), where the measured velocity signals are used in the feedback for damping control. In order to show the advantage and effectiveness of the 3-D sensor, Fig. 10(b) is the vibration system without the 3-D sensor system, where the corresponding relative velocity signals (with respect to the base) are used instead.

As shown in Fig. 10(a), the control signals u_{1x} and u_{1y} are the linear functions of the relative velocity signals which can be expressed as

$$u_{1x} = \alpha_1 \dot{\hat{x}}_2 \quad (28)$$

$$u_{1y} = \alpha_2 \dot{\hat{y}}_2 \quad (29)$$

where α_1 and α_2 are the dimensionless feedback control strength. According to the modeling analysis above, the

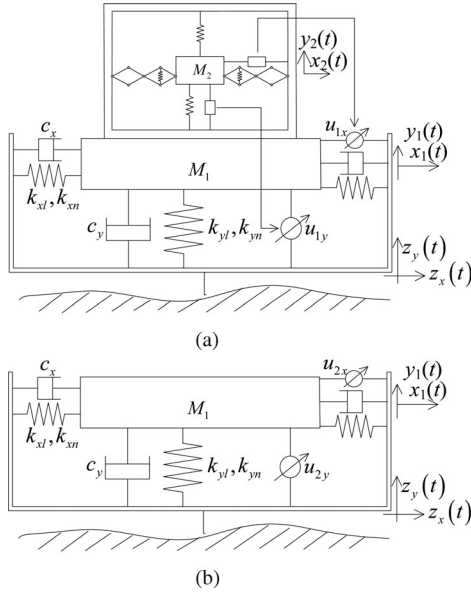


Fig. 10. Structural diagram of the vibration system in two directions with linear feedback control. Plot (a) is with the 3-D sensor and (b) is without the 3-D sensor.

dimensionless dynamic equation of the vibration system is as

$$\begin{aligned} \hat{x}_1'' + 2\hat{x}_1 + 2\gamma_x \hat{x}_1^3 + \gamma_1 \left(\frac{\lambda_s \sec^3 \theta}{ln^2} - \frac{2 \tan^2 \theta}{n^2} \right) \hat{x}_2 + 4\xi_x \hat{x}_1' \\ + \left[\gamma_1 \sec^6 \theta \left(\frac{3 - 2 \cos 2\theta}{4l^2 n^4} \right) \left(\frac{\lambda_s \sec \theta}{2l} - 1 \right) - \frac{\gamma_2}{l_{20}^2} \right] \hat{x}_2^3 \\ + \left[\frac{2\gamma_2}{l_{20}^2} - \frac{\gamma_1 (2l \cos \theta - \lambda_s) (2 - \cos 2\theta) \sec^5 \theta}{8l^3 n^4} \right] \hat{x}_2 \hat{y}_2^2 \\ = u_{1x} - z_x'' = \alpha_1 \hat{x}_2' - z_x'' \end{aligned} \quad (30)$$

$$\begin{aligned} \hat{y}_1'' + \omega_y^2 \hat{y}_1 + \gamma_y \hat{y}_1^3 + \left(\frac{\gamma_1 \lambda_s \sec \theta}{ln^2} - 2\gamma_2 \right) \hat{y}_2 \\ + \left[\frac{2\gamma_2}{l_{20}^2} - \frac{\gamma_1 (2l \cos \theta - \lambda_s) (2 - \cos 2\theta) \sec^5 \theta}{8l^3 n^4} \right] \hat{x}_2^2 \hat{y}_2 \\ + 2\xi_y \hat{y}_1' + \frac{\gamma_1 \sec^2 \theta}{4l^2 n^4} \left(\frac{\lambda_s \sec \theta}{2l} - 1 \right) \hat{y}_2^3 = u_{1y} - z_y'' \\ = \alpha_2 \hat{y}_2' - z_y'' \end{aligned} \quad (31)$$

For harmonic excitation of the base, the displacement transmissibility in the two directions can be defined as

$$T_{vx} = \|x_1\| / \|z_x\| \quad (32)$$

$$T_{vy} = \|y_1\| / \|z_y\|. \quad (33)$$

The results with the 3-D sensor are shown in Fig. 11.

Fig. 11 reveals that increasing the feedback control strength can reduce the vibration response of the mass M_1 in the two directions both in low- and high-frequency range; the signals measured by the 3-D sensor are actually the absolute motion/velocity of the vibrating mass.

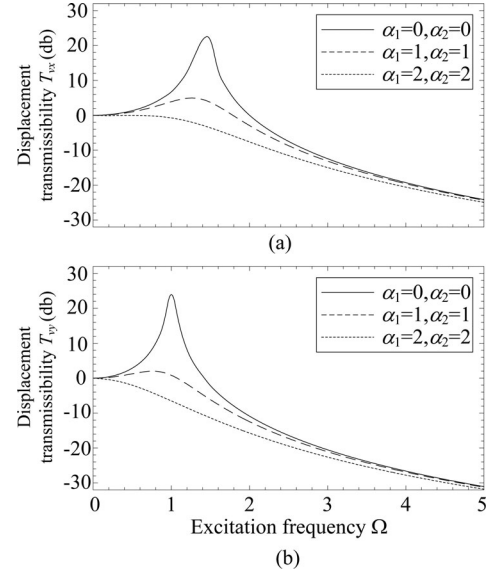


Fig. 11. Displacement transmissibility of M_1 by feedback control signals from the 3DS. Plot (a) is T_{vx} and (b) is T_{vy} .

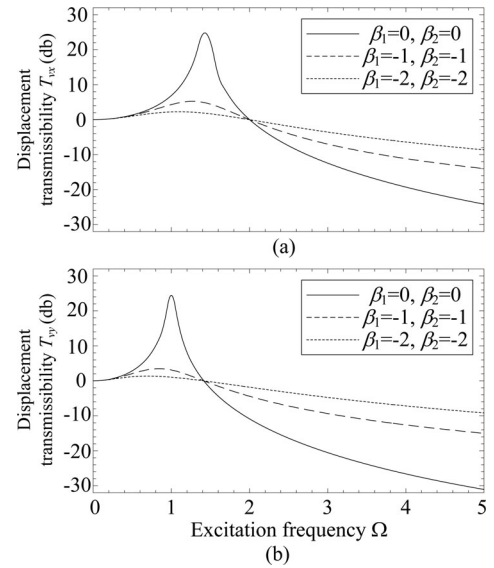


Fig. 12. Displacement transmissibility of M_1 by relative velocity control signal. Plot (a) is T_{vx} and (b) is T_{vy} .

Similarly, in Fig. 10(b), the feedback control signals u_{2x} and u_{2y} in the two directions are the linear functions of the relative velocity of M_1 with respect to the base which are

$$u_{2x} = \beta_1 \hat{x}_1' \quad (34)$$

$$u_{2y} = \beta_2 \hat{y}_1'. \quad (35)$$

Then, the dimensionless dynamic equation of the vibration object with feedback control in Fig. 10(b) is given as

$$\hat{x}_1'' + 2\hat{x}_1 + 2\gamma_x \hat{x}_1^3 + 4\xi_x \hat{x}_1' = u_{2x} - z_x'' = \beta_1 \hat{x}_1' - z_x'' \quad (36)$$

$$\hat{y}_1'' + \omega_y^2 \hat{y}_1 + \gamma_y \hat{y}_1^3 + 2\xi_y \hat{y}_1' = u_{2y} - z_y'' = \beta_2 \hat{y}_1' - z_y''. \quad (37)$$

The results with the relative velocity feedback control (i.e., without the 3-D sensor) are shown in Fig. 12.

From Fig. 12, it can be seen that using the relative velocity between the vibrations of mass M_1 and the base can reduce the resonant peak while it increases the vibration response in high-frequency range. Obviously, the proposed 3-D sensor provides an effective way to measure absolute motion states for feedback control which would definitely benefit various engineering practices.

V. CONCLUSION

This study proposes a novel 3-D sensor which can obtain absolute motion states of a vibration system subjected to different types of base excitations. By employing horizontally predeformed SLSs, the 3-D sensor system has QZS in three directions. This provides relatively a fixed point in a vibration system, which can thus be utilized for absolute motion measurement for different purposes in various engineering practices (robust control, vibration control, filter design, signal processing, etc.). Because the structural parameters in the sensor system can be easily adjusted to ensure the QZS property, the sensor system with SLSs has excellent vibration isolation effect in a large frequency range. This results in the vibration of the sensor mass much smaller than the sensor platform. Thus, the measured signals (relative motion) can be used to represent absolute motions with sufficient accuracy by adjusting the structure parameters. Both theoretical analysis and simulation or example studies demonstrate clearly the effectiveness of this novel sensor system for different vibration sources including periodic and random excitations.

Further study will focus on a practical experimental validation and prototyping of the proposed 3-D sensor system and its applications.

APPENDIX

TABLE I
STRUCTURAL PARAMETERS OF THE SYSTEM WITH DEFAULT VALUES

Symbol	Structural parameters	Unit	Default values
M_1	Mass of vibration object	kg	2
M_2	Mass in 3-D sensor	kg	0.2
k_{xl}	Linear stiffness of horizontal springs	N·m ⁻¹	2000
k_{xn}	Nonlinear stiffness of horizontal springs	N·m ⁻³	10 000
k_{yl}	Linear stiffness of vertical spring	N·m ⁻¹	2000
k_{yn}	Nonlinear stiffness of vertical spring	N·m ⁻³	10 000
c_x	Damping coefficient in horizontal direction	N·s·m ⁻¹	3
c_y	Damping coefficient in vertical direction	N·s·m ⁻¹	5
k_1	Stiffness of spring in SLS	N·m ⁻¹	300
l_{10}	Original length of springs in SLSs	m	
k_2	Vertical spring stiffness	N·m ⁻¹	100
l_{20}	Original length of vertical spring in 3-D sensor	m	0.5
N	Number of layer of SLS		1
L	Length of rod in SLS	m	0.2
θ	Assembly angle of rod	rad	0.6155
λ_s	Predeformation of horizontal spring	m	0.109

TABLE II
BASE EXCITATIONS, ABSOLUTE MOTIONS, AND RELATIVE MOTIONS OF THE VIBRATION SYSTEM IN FIG. 1

Symbol	Structural parameters	Unit
x_1	Horizontal absolute displacement of M_1	m
y_1	Vertical absolute displacement of M_1	m
x_2	Horizontal absolute displacement of M_2	m
y_2	Vertical absolute displacement of M_2	m
\hat{x}_1	Horizontal relative displacement of M_1 to base	m
\hat{y}_1	Vertical relative displacement of M_1 to base	m
\hat{x}_2	Horizontal relative displacement of M_2 to M_1	m
\hat{y}_2	Vertical relative displacement of M_2 to M_1	m
z_x	Horizontal base excitation	m
z_y	Vertical base excitation	m
ω	Frequency of harmonic excitation	rad·s ⁻¹
z_{x0}	Amplitude of horizontal excitation z_x	m
z_{y0}	Amplitude of vertical excitation z_y	m

TABLE III
EXPRESSIONS AND VALUES OF DIMENSIONLESS PARAMETERS IN (8)–(11)

Symbol	Expressions	Values
ω_y	$\sqrt{\frac{k_{yl}}{k_{xl}}}$	1
γ_x	$\frac{k_{xn}}{k_{xl}}$	5
γ_y	$\frac{k_{yn}}{k_{xl}}$	5
ξ_x	$\frac{c_x}{2\sqrt{M_1 k_{xl}}}$	0.0237
ξ_y	$\frac{c_y}{2\sqrt{M_1 k_{xl}}}$	0.0395
γ_1	$\frac{k_1}{k_{xl}}$	0.15
γ_2	$\frac{k_2}{k_{xl}}$	0.05
μ	$\frac{M_1}{M_2}$	10
Ω	$\frac{\omega}{\omega_0}$	$\frac{\omega}{\sqrt{1000}}$

REFERENCES

- [1] T. B. Schon, A. Wills, and B. Ninness, "System identification of nonlinear state-space models," *Automatica*, vol. 47, no. 1, pp. 39–49, Jan. 2011.
- [2] P. B. Schmidt and R. D. Lorenz, "Design principles and implementation of acceleration feedback to improve performance of DC drives," *IEEE Trans. Ind. Appl.*, vol. 28, no. 3, pp. 594–599, May/Jun. 1992.
- [3] A. Benallegue, A. Mokhtari, and L. Fridman, "High-order sliding-mode observer for a quadrotor UAV," *Int. J. Robust Nonlinear Control*, vol. 18, no. 4–5, pp. 427–440, Mar. 2008.
- [4] A. J. Calise, N. Hovakimyan, and M. Idan, "Adaptive output feedback control of nonlinear systems using neural networks," *Automatica*, vol. 37, no. 8, pp. 1201–1211, Aug. 2001.
- [5] B. Aldiwi and H. K. Khalil, "Robust adaptive output feedback control of nonlinear systems without persistence of excitation," *Automatica*, vol. 33, no. 11, pp. 2025–2032, Nov. 1997.
- [6] T. Umeno and Y. Hori, "Robust speed control of DC servomotors using modern two-degrees-of-freedom controller Design," *IEEE Trans. Ind. Electron.*, vol. 38, no. 5, pp. 363–368, Oct. 1991.
- [7] W. C. Sun, H. J. Gao, and O. Kaynak, "Adaptive backstepping control for active suspension systems with hard constraints," *IEEE Trans. Mechatronics*, vol. 18, no. 3, pp. 1072–1079, Jun. 2013.
- [8] X. J. Jing and L. Cheng, "An optimal-PID control algorithm for training feedforward neural networks," *IEEE Trans. Ind. Electron.*, vol. 60, no. 6, pp. 2273–2283, Jun. 2013.
- [9] H. Y. Li, X. J. Jing, and H. R. Karimi, "Output-feedback based H ∞ control for vehicle suspension systems with control delay," *IEEE Trans. Ind. Electron.*, vol. 61, no. 1, pp. 436–446, Jan. 2013.

- [10] H. Y. Li, H. H. Liu, H. J. Gao, and P. Shi, "Reliable fuzzy control for active suspension systems with actuator delay and fault," *IEEE Trans. Fuzzy Syst.*, vol. 20, no. 2, pp. 342–357, Apr. 2012.
- [11] X. C. Zhu, X. J. Jing, and L. Cheng, "Magnetorheological fluid dampers: A review on structure design and analysis," *J. Intell. Mater. Syst. Struct.*, vol. 23, no. 8, pp. 839–837, Mar. 2012.
- [12] Y. Maeda and M. Iwasaki, "Circle condition-based feedback controller design for fast and precise positioning," *IEEE Trans. Ind. Electron.*, vol. 61, no. 2, pp. 1113–1122, Feb. 2014.
- [13] R. C. Luo, "Sensor technologies and microsensor issues for mechatronics systems," *IEEE Trans. Mechatronics*, vol. 1, no. 1, pp. 39–49, Mar. 1996.
- [14] G. A. Bertone, Z. H. Meiksin, and M. L. Carroll, "Investigation of a capacitance-based displacement transducer," *IEEE Trans. Instrum. Meas.*, vol. 39, no. 2, pp. 424–428, Apr. 1990.
- [15] N. Yazdi, F. Ayazi, and K. Najafi, "Micromachined inertial sensors," *Proc. IEEE*, vol. 86, no. 8, pp. 1640–1659, Aug. 1998.
- [16] G. T. Capraro, A. Farina, H. Griffiths, and M. C. Wicks, "Knowledge-based radar signal and data processing: A tutorial review," *IEEE Signal Process. Mag.*, vol. 23, no. 1, pp. 18–29, Jan. 2006.
- [17] M. G. Allen, "Diode laser absorption sensors for gas-dynamic and combustion flows," *Meas. Sci. Technol.*, vol. 9, no. 4, pp. 545–562, Apr. 1998.
- [18] S. Donati, L. Falzoni, and S. Merlo, "A PC-interfaced, compact laser-diode feedback interferometer for displacement measurements," *IEEE Trans. Instrum. Meas.*, vol. 45, no. 6, pp. 942–947, Dec. 1996.
- [19] S. Donati, G. Giuliani, and S. Merlo, "Laser diode feedback interferometer for measurement of displacements without ambiguity," *IEEE J. Quantum Electron.*, vol. 31, no. 1, pp. 113–119, Jan. 1995.
- [20] J. P. Richard, "Time-delay systems: An overview of some recent advances and open problems," *Automatica*, vol. 39, no. 10, pp. 1667–1694, Oct. 2003.
- [21] A. Bellen, N. Guglielmi, and A. E. Ruehli, "Methods for linear systems of circuit delay differential equations of neutral type," *IEEE Trans. Circuits Syst. I, Fundam. Theory Appl.*, vol. 46, no. 1, pp. 201–215, Jan. 1999.
- [22] X. L. Luan, S. Peng, and F. Lin, "Stabilization of networked control system with random delay," *IEEE Trans. Ind. Electron.*, vol. 58, no. 9, pp. 4323–4330, Sep. 2011.
- [23] G. D. Hu and T. Mitsui, "Stability analysis of numerical methods for systems of neutral delay-differential equations," *BIT Numerical Math.*, vol. 35, no. 4, pp. 504–515, Jun. 1995.
- [24] Y. Y. Zhao and J. Xu, "Effects of delayed feedback control on nonlinear vibration absorber system," *J. Sound Vib.*, vol. 308, pp. 212–230, Nov. 2007.
- [25] N. Olgac and B. T. Holm-Hansen, "A novel active vibration absorption technique: delayed resonator," *J. Sound Vib.*, vol. 176, pp. 93–104, Sep. 1994.
- [26] L. L. Chung, C. C. Lin, and S. Y. Chu, "Optimal direct output feedback of structural control," *J. Eng. Mech.*, vol. 119, no. 11, pp. 2157–2173, Jan. 1993.
- [27] X. T. Sun, X. J. Jing, J. Xu, and L. Cheng, "Vibration isolation via a scissor-like structured platform," *J. Sound Vib.*, vol. 333, no. 9, pp. 2404–2420, Apr. 2014.
- [28] I. Kovacic, M. J. Brennan, and B. Linetou, "Effect of a static force on the dynamic behavior of a harmonically excited quasi-zero stiffness system," *J. Sound Vib.*, vol. 325, pp. 870–883, Jun. 2009.
- [29] T. D. Le and K. K. Ahn, "A vibration isolation system in low frequency excitation region using negative stiffness structure for vehicle seat," *J. Sound Vib.*, vol. 330, no. 26, pp. 6311–6335, Dec. 2011.
- [30] A. Carrella, M. J. Brennan, T. P. Waters, and V. Lopes, Jr., "Force and displacement transmissibility of a nonlinear isolator with high-static-low-dynamic-stiffness," *Int. J. Mech. Sci.*, vol. 55, no. 1, pp. 22–29, Feb. 2012.
- [31] X. Jing, "Nonlinear characteristic output spectrum for nonlinear analysis and design," *IEEE/ASME Trans. Mechatronics*, vol. 19, no. 1, pp. 171–183, Feb. 2014.
- [32] A. A. Eielson, M. Vagia, J. T. Gravdahl, and K. Y. Pettersen, "Damping and tracking control schemes for nanopositioning," *IEEE/ASME Trans. Mechatronics*, vol. 19, no. 2, pp. 432–444, Apr. 2014.
- [33] J. Yao, Z. Jiao, D. Ma, and L. Yan, "High-accuracy tracking control of hydraulic rotary actuators with modeling uncertainties," *IEEE/ASME Trans. Mechatronics*, vol. 19, no. 2, pp. 633–641, Apr. 2014.
- [34] H. R. Harrison, *Advanced Engineering Dynamics*. New York, NY, USA: Wiley, 1997.



Xiuting Sun was born in Shanghai, China, in August 1987. She received the B.Eng. degree in mechanics from Tongji University, Shanghai, China, in 2009. She is currently working toward a dual degree with The Hong Kong Polytechnic University, Hung Hom, Hong Kong, and the Ph.D. degree with Tongji University.

Her research interest includes nonlinear isolator.



Xingjian Jing (M'13) received the B.S. degree from Zhejiang University, Hangzhou, China, in 1998; the M.S. degree in intelligent systems and control, and the Ph.D. degree in mechatronics from the Shenyang Institute of Automation, Chinese Academy of Sciences, Shenyang, China, in 2001 and 2005, respectively. He received the Ph.D. degree in nonlinear systems and signal processing from the Department of Automatic Control and Systems Engineering, University of Sheffield, Sheffield, U.K., in 2008.

He is currently an Assistant Professor with the Department of Mechanical Engineering, The Hong Kong Polytechnic University (PolyU), Hung Hom, Hong Kong. Before joining PolyU in November 2009, he was a Research Fellow with the Institute of Sound and Vibration Research, University of Southampton, working on biomedical signal processing. His current research interests include nonlinear analysis and design in the frequency domain; system identification, signal processing and control of complex nonlinear systems; intelligent computing methods; and their applications in nonlinear mechanical systems (sound and vibration control), nonlinear physiological systems (neural systems), and robotic systems.

Dr. Jing is an active reviewer for many known journals and conferences, and also serves in technical/editorial boards of several international journals/conferences.



Li Cheng received the B.S. degree in applied mechanics from Xi'an Jiaotong University, Xi'an, Shaanxi, China, in 1984; and the DEA and Ph.D. degrees from the Institut National des Sciences Appliquées de Lyon (INSA-Lyon), Villeurbanne Cedex, France, in 1986 and 1989, respectively.

He joined Laval University in Canada as an Assistant Professor in the Department of Mechanical Engineering, in 1992. In the following years, he was promoted to Associate Professor and Full Professor, before joining the Department of Mechanical Engineering, The Hong Kong Polytechnic University, in 2000. He is currently a Chair Professor and the Director of the Consortium for Sound and Vibration Research. His research interests include noise and vibration control, fluid–structure interaction, damage detection, and smart material/structure.

Prof. Cheng has been a member of the board of directors and committees of different learning organizations such as Acoustical Society of America, Canadian Acoustical Society, Acoustical Society of China, and Chinese Society of Noise and Vibration Engineering. He also serves in the editorial boards or advisory committee for several international journals.



Jian Xu was born in Shanghai, China, on December 27, 1961. He received the Ph.D. degree in dynamics and control from Tianjin University, Tianjin, China, in 1994.

Since 2000, he has been a Professor at the School of Aerospace Engineering and Applied Mechanics, Tongji University. His research interests include delay-induced dynamics, nonlinear dynamics and control, stability, bifurcation and chaos in nature and engineering, neural networks with delayed connection, and biology systems.